

AnomalyControl: Learning Cross-modal Semantic Features for Controllable Anomaly Synthesis

Shidan He¹, Lei Liu^{2,3}, Shen Zhao^{1,†}
¹Sun Yat-sen University, ²CUHK-Shenzhen, ³Ant Group
zhaosh35@mail.sysu.edu.cn

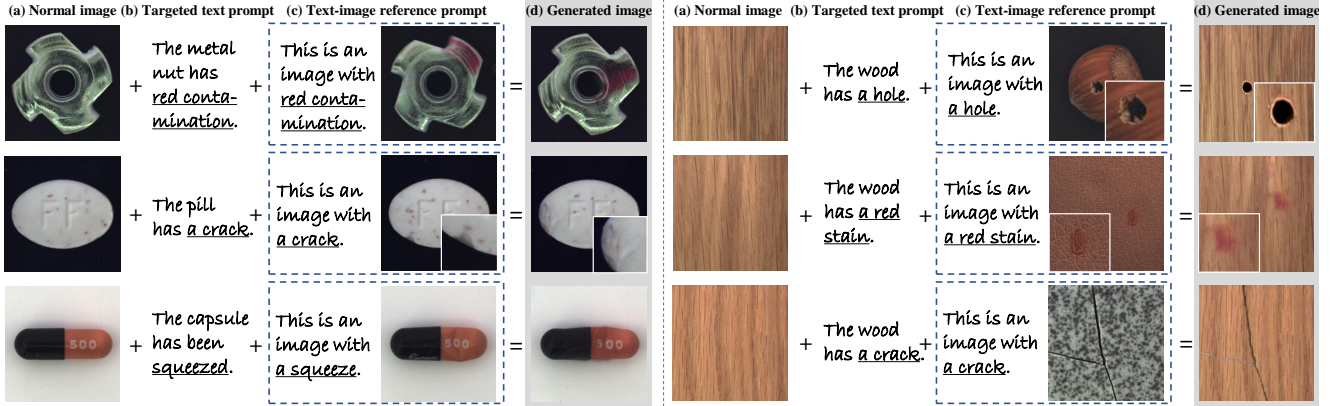


Figure 1. Learning cross-modal semantic features as the prior, our method can achieve both **realism** and **generalization** for controllable anomaly synthesis. **Realism:** The targeted text prompt provides a full description for the targeted anomaly image to be generated (e.g., color, texture, and shape), while the text-image reference prompt provides a template reference for the targeted anomaly region (e.g., magnified area). **Generalization:** Our method does not require the matched pair of text-image reference prompt and targeted text prompt, e.g., the text-image reference can exhibit a different material surface compared with the targeted text prompt (e.g., the right examples).

Abstract

Anomaly synthesis is a crucial approach to augment abnormal data for advancing anomaly inspection. Based on the knowledge from the large-scale pre-training, existing text-to-image anomaly synthesis methods predominantly focus on textual information or coarse-aligned visual features to guide the entire generation process. However, these methods often lack sufficient descriptors to capture the complicated characteristics of realistic anomalies (e.g., the fine-grained visual pattern of anomalies), limiting the realism and generalization of the generation process. To this end, we propose a novel anomaly synthesis framework called AnomalyControl to learn cross-modal semantic features as guidance signals, which could encode the generalized anomaly cues from text-image reference prompts and improve the realism of synthesized abnormal samples. Specifically, AnomalyControl adopts a flexible and non-matching prompt pair (i.e., a text-image reference prompt and a targeted text prompt)¹, where a Cross-modal Semantic Modeling (CSM) module is designed to extract cross-modal se-

mantic features from the textual and visual descriptors. Then, an Anomaly-Semantic Enhanced Attention (ASEA) mechanism is formulated to allow CSM to focus on the specific visual patterns of the anomaly, thus enhancing the realism and contextual relevance of the generated anomaly features. Treating cross-modal semantic features as the prior, a Semantic Guided Adapter (SGA) is designed to encode effective guidance signals for the adequate and controllable synthesis process. Extensive experiments indicate that AnomalyControl can achieve state-of-the-art results in anomaly synthesis compared with existing methods while exhibiting superior performance for downstream tasks.

1. Introduction

Anomaly inspection plays a crucial role in various fields, from industrial anomaly detection [17, 38] to medical imaging [14]. One of the most challenging issues is the scarcity of diverse abnormal data due to the resource-intensive procedure for acquiring large and varied datasets. Therefore, anomaly synthesis task [7, 8, 12, 13, 21, 22, 34, 35, 39] gradually emerged as an advancing technique to improve the data scale of the available abnormal sample.

¹Non-matching: the text-image reference prompt and targeted text prompt are only required to describe the same anomaly type without needing to match in surface details or materials.

Many downstream tasks, such as anomaly detection and localization, could benefit from enriching the training dataset using synthetic anomaly samples. Recently, text-to-image synthesis techniques [26, 31] have received more research attention for their outperforming performance, which can generate visually realistic natural images according to the input text prompt. However, for the anomaly synthesis task, they still suffer from insufficient descriptors of the textual prompt, resulting in unsatisfactory realism for the generated anomalies. This limitation hampers the model’s ability to recognize rare or previously unseen defect types.

Motivated by the success of publicly available large text-to-image diffusion models [2, 20, 27, 29, 32], many approaches proposed to incorporate extra control signals to assist the diffusion process, which could enrich the targeted text prompt via injecting more prior information. For example, ControlNet [37], Uni-ControlNet [40], and IP-Adapter [33] proposed to apply adapters on stable diffusion models [27] to provide extra control for generation. The main idea is to learn stylistic information from a reference image (called image prompt). However, image prompts without a clear focal point generally offer weak alignment signals, limiting the effectiveness of generating high-fidelity and customized images. This limitation is especially pronounced in anomaly synthesis tasks, where anomalies typically occupy only a small region of the image and can easily be overlooked during generation. As a result, the synthesized anomalies often lack sufficient details to match real samples, failing to meet the high precision required for effective anomaly inspection and resulting in a lack of realism in the synthesized samples.

To this end, this work aims to enhance the controllability of anomaly synthesis, improving the realism of synthesized samples and supporting more flexible and generalizable prompts. The resulting framework is called AnomalyControl (as shown in Figure 2). Specifically, the controllability signals come from a non-matching pair, *i.e.*, a text-image reference prompt and a targeted text prompt. The text-image reference prompt includes a textual anomaly descriptor and visual anomaly descriptor, which are used to offer semantic and contextual cues for guiding the synthesis process. Importantly, the anomaly described by the text-image reference prompt is aligned with that indicated in the targeted text prompt, while the background and other properties are left unrestricted, allowing for greater flexibility in anomaly placement. To improve realism, we introduce Cross-modal Semantic Modeling (CSM) to capture cross-modal semantic features via multimodal interactions, where the Anomaly-Semantic Enhanced Attention (ASEA) mechanism could extract fine-grained information related to the anomaly region. By taking cross-modal semantic features as the prior, the Semantic Guided Adapter (SGA) could in-

sert effective semantic signals to support an adequate and controllable synthesis process. Table 1 makes a comparison between AnomalyControl and previous methods, where our method exhibits several advantages in terms of realism, generalization, plug-and-play functionality, and controllability.

In summary, our contributions are as follows:

- A novel framework called AnomalyControl is proposed to achieve controllable anomaly synthesis in a flexible manner, which can generate realistic and generalized anomaly samples guided by a non-matching pair.
- We design a Cross-modal Semantic Modeling (CSM) module to extract cross-modal semantic features from the textual and visual anomaly descriptors, where an Anomaly-Semantic Enhanced Attention (ASEA) mechanism can encode fine-grained visual details into cross-modal semantic features via multimodal interactions, which could further improve the realism of generated anomalies.
- We formulate a Semantic Guided Adapter (SGA) allowing cross-modal semantic features to pass through the generation procedure (*i.e.*, diffusion process), providing adequate and controllable synthesis instructions to generate high-quality anomalies.
- Extensive experiments demonstrate that our method can generate realistic and generalized anomalies based on different control signals (as shown in Figure 1) and significantly enhance anomaly inspection performance.

2. Related Work

2.1. Anomaly Synthesis

Anomaly synthesis has become an essential technique to support anomaly detection systems, especially in scenarios where real defect data is scarce. Existing methods can be broadly divided into two main categories. First, crop-and-paste anomaly augmentation methods [7, 34] combine normal images with abnormal patterns sourced from small abnormal samples or external textures. While these methods are computationally efficient and straightforward to implement, they often lack realism and generalization, limiting their ability to represent the complex characteristics of anomalies. Second, generative model-based methods [8, 12, 13, 21, 22, 35, 39], such as GANs and diffusion models, generate anomalies from scratch or by fine-tuning pre-trained models. Although these methods typically perform well for in-distribution anomalies, they require sufficient sample generalization and frequently struggle to produce out-of-distribution anomalies, which limits their ability to generalize to unseen defect types.

2.2. Text-to-Image Diffusion Models

Since fine-tuning large pre-trained models is often inefficient, using adapters has become a more efficient alterna-

Table 1. Comparisons with previous methods. **Realism** refers to the ability to generate realistic anomaly images with complex and fine-grained details. **Generalization** indicates the capability to transfer anomaly features across different objects and surfaces, allowing the model to generate diverse anomalies beyond the knowledge learned from pre-training. Anomaly synthesis methods could prioritize high-fidelity anomaly data for downstream tasks, where the generalization ability is limited by the knowledge learned from pre-training. Benefiting from large-scale pre-training, image generation methods dominate the slightly stronger generalization ability for natural images, but they still suffer from low-quality anomaly synthesis due to the complicated characteristics of anomalies. Our AnomalyControl can perform well for realism and generalization, along with plug-and-play flexibility and controllability.

Method	Venue	Task	Realism	Generalization	Plug-and-Play	Controllability
DRAEM [34]	ICCV’21	Anomaly Synthesis			✓	
DefGAN [35]	WACV’21	Anomaly Synthesis	✓			
DFMGAN [8]	AAAI’23	Anomaly Synthesis	✓			
AnoDiff [13]	AAAI’24	Anomaly Synthesis	✓			
AnoXFusion [12]	Arxiv’24	Anomaly Synthesis	✓			
ControlNet [37]	ICCV’23	Image Generation		✓	✓	✓
Uni-ControlNet [40]	NeurIPS’23	Image Generation		✓	✓	✓
IP-Adapter [33]	Arxiv’23	Image Generation		✓	✓	✓
AnomalyControl		Anomaly Synthesis	✓	✓	✓	✓

tive. Adapters introduce a small number of trainable parameters into the original model while freezing the pre-trained weights, significantly reducing training costs. With the success of large text-to-image diffusion models like DALL-E 2 [26], Imagen [29], and Stable Diffusion [27], significant progress has been made in image generation. However, writing complex text prompts remains a challenge, and pure text often fails to fully express complex scenes or concepts. To address this, methods such as ControlNet [37] and Uni-ControlNet [40] have introduced lightweight adapters in pre-trained Stable Diffusion models, enabling more precise control by incorporating additional prompts, such as structural or image-based control. IP-Adapter [33] further optimizes this approach by introducing a decoupled cross-attention mechanism, improving the effectiveness of image prompting, and even achieving performance comparable to fine-tuning the entire model. However, image prompts without a clear focus often provide weak alignment signals, making it difficult to generate high-fidelity, customized images, especially in anomaly synthesis, where anomalies are small and easily overlooked.

3. Methods

3.1. Preliminaries

Stable Diffusion. Our method is built upon Stable Diffusion [27], which efficiently performs the diffusion process in a low-dimensional latent space instead of pixel space by using an auto-encoder [15]. Specifically, given an input image $x_i \in \mathbb{R}^{H \times W \times 3}$, the encoder maps it to a latent representation $z_0 = \xi(x_i)$, where $z_0 \in \mathbb{R}^{h \times w \times c}$ with $H/h = W/w$ as the downsampling factor and c as the number of latent dimensions. The diffusion process utilizes a denoising UNet [28] to gradually refine a noisy latent z_t , conditioned on the current timestep T and a textual prompt embedding

C . Here, C represents the embedding of the targeted text prompt, generated by a pre-trained CLIP [25] text encoder. The training objective is defined as:

$$\mathcal{L} = \mathbb{E}_{z_t, t, C, \epsilon \sim \mathcal{N}(0, 1)} [\|\epsilon - \epsilon_\theta(z_t, t, C)\|_2^2], \quad (1)$$

where the goal is to predict and remove the noise ϵ added to z_t at each timestep.

Overall Framework. The pipeline of AnomalyControl is illustrated in Figure 2. Our framework consists of two main modules: Cross-modal Semantic Modeling (CSM) and Semantic Guided Adapter (SGA). Given the text-image reference prompts as the input, *i.e.*, a visual anomaly descriptor I_a and textual anomaly descriptor T_a as the reference, CSM module aims to extract fine-grained cross-modal semantic features by integrating both text and image information using a vision-language model (VLM). An Anomaly-Semantic Enhanced Attention (ASEA) is introduced to refine the attention process in VLM, ensuring that the model can focus on the specific visual patterns of the anomaly, thus enhancing the realism and contextual relevance of the generated anomaly features. The SGA then introduces these enriched cross-modal semantic features as priors into the diffusion process, allowing flexible control over anomaly characteristics. Together, these components ensure that generated anomalies are realistic and contextually aligned with descriptive cues. The detailed training algorithm of our AnomalyControl is outlined in Algorithm 1.

3.2. AnomalyControl

3.2.1. Cross-modal Semantic Modeling

Leveraging the text-image reference prompt, the CSM module targets to encode sufficient cross-modal reference infor-

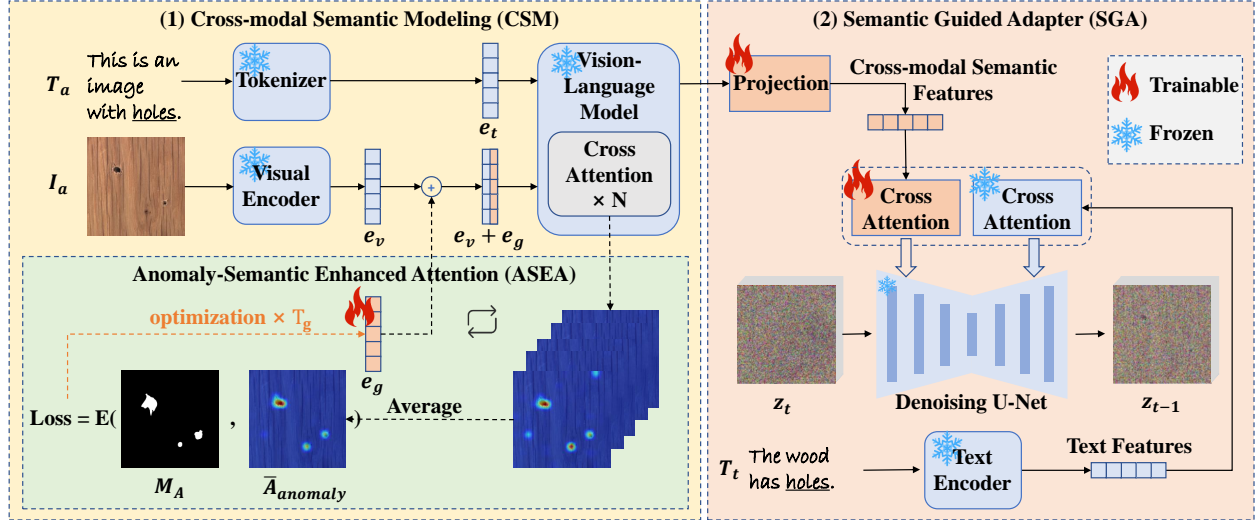


Figure 2. Overall pipeline of the proposed AnomalyControl. Our framework consists of three main modules to enhance controllability in anomaly synthesis. (1) **Cross-modal Semantic Modeling (CSM)** integrates both visual anomaly descriptors I_a and textual anomaly descriptors T_a to capture precise cross-modal semantic features using a frozen vision-language model (VLM). (2) **Anomaly-Semantic Enhanced Attention (ASEA)** employ a trainable attention guidance variable e_g to emphasize the designated anomaly regions, which can capture more accurate semantic information without retraining the frozen VLM. (3) **Semantic Guided Adapter (SGA)** utilizes a decoupled cross-attention to support controllable anomaly synthesis, allowing for a flexible and generalized generation.

mation as control signals for the diffusion process, *i.e.*, consistent anomaly semantics from the text-image prompt.

Specifically, the text-image reference prompt provides a visual anomaly descriptor I_a and a textual anomaly descriptor T_a . Note that such text-image reference prompt only focuses on the contextual and descriptive information of the anomaly region, excluding the anomaly-unrelated information, such as background and materials. Such a pattern would allow greater flexibility in anomaly placement. In detail, I_a defines a specific anomaly pattern to provide a direct visual context reference, ensuring accurate visual control over the generated anomaly. T_a is created by combining an anomaly-specific keyword K with a template, providing semantic guidance to help the model generate samples that accurately reflect the designated anomaly type and attributes. The anomaly described in the T_a aligns with the anomaly region in the I_a , while the background and other elements of I_a remain unconstrained.

To capture effective cross-modal information from the text-image reference, a frozen VLM with cross-attention layers is utilized for its powerful multimodal integration ability. Thus, VLM-based CSM could integrate the reference image and text to obtain a unified semantic feature for the anomaly, called a cross-modal semantic feature, which serves as a prior for the following diffusion process. Natural needs arise from the anomaly-specific regions without losing fine-grained detail to generate realistic and contextually accurate anomalies, which motivates the introduction of the

ASEA mechanism in the following section.

3.2.2. Anomaly-Semantic Enhanced Attention

ASEA forces the CSM's attention to focus on designated anomaly regions within the image reference, enabling precise extraction of anomaly-specific features for high-fidelity synthesis. The main pathway is to isolate the anomaly region in the attention map and optimize a trainable attention guidance variable, e_g , which assists the frozen VLM in prioritizing relevant anomaly areas without retraining steps.

The textual anomaly descriptor T_a is structured as the template of “*This is an image with [anomaly]*”, where the variable *[anomaly]* specifies the anomaly type. L_{prefix} represents the length of the fixed prefix “*This is an image with*”. L denotes the total length of T_a . The anomaly descriptor *[anomaly]* begins at position $L_{\text{prefix}} + 1$ and extends to L .

Firstly, an attention map A is generated by the VLM's cross-attention layer, focusing on the feature span A_{anomaly} associated with the *[anomaly]* part of the text prompt. A_{anomaly} captures the anomaly-specific attention values: $A_{\text{anomaly}} = A[L_{\text{prefix}} + 1 : L, :]$. By averaging these values across the anomaly section, we compute a mean attention map, \bar{A}_{anomaly} , which helps stabilize the focus by reducing noise from individual tokens:

$$\bar{A}_{\text{anomaly}} = \frac{1}{L - L_{\text{prefix}}} \sum_{i=L_{\text{prefix}}+1}^L A[i, :], \quad (2)$$

To further refine the attention on anomaly regions, we

apply an anomaly region mask M_A to \bar{A}_{anomaly} . This mask constrains attention to the spatial area of interest in the image, which is enhanced by introducing the trainable attention guidance variable e_g . The optimization of e_g is guided by an energy function [6], defined as:

$$E(\bar{A}_{\text{anomaly}}, M_A) = \left(1 - \frac{\sum_{i \in M_A} \bar{A}_{\text{anomaly},i}}{\sum_i \bar{A}_{\text{anomaly},i}} \right)^2, \quad (3)$$

where $i \in M_A$ refers to indices within the masked region. This function encourages concentration within M_A , prioritizing relevant features in the anomaly area.

Finally, e_g is optimized iteratively over T_g steps using gradient descent to minimize the energy function:

$$e_g \leftarrow e_g - \alpha \nabla_{e_g} E(\bar{A}_{\text{anomaly}}, M_A), \quad (4)$$

where α is the learning rate. Through this iterative refinement, ASEA aligns the model’s attention precisely with M_A , effectively capturing anomaly-specific details. The challenge here lies in maintaining focused attention on the anomaly regions without disrupting the model’s overall comprehension, a task ASEA addresses by carefully guiding attention with e_g .

3.2.3. Semantic Guided Adapter

Motivated by the decoupled cross-attention [33], the SGA module introduces an adaptive mechanism to incorporate an additional targeted text prompt T_t as input, indicating the specific anomaly to be generated. Unlike previous approaches using solely image features as the prior [33, 40], which often miss critical details in subtle anomaly regions with low signal-to-noise ratios, SGA relies on a richer, semantically focused representation, *i.e.*, cross-modal semantic features produced by CSM, which captures fine-grained anomaly details essential for accurate synthesis.

To facilitate classifier-free guidance [11], similar to text conditioning, SGA employs random dropout during training. This process involves occasionally setting cross-modal semantic features to zero, allowing the model to jointly learn both conditional and unconditional prompts. The enhanced cross-attention mechanism for integrating text and cross-modal semantic features is defined as:

$$Z_{\text{new}} = \mathcal{S} \left(\frac{Q(K)^T}{\sqrt{d}} \right) V + \gamma \cdot \mathcal{S} \left(\frac{Q(K')^T}{\sqrt{d}} \right) V', \quad (5)$$

where γ is a weight to balance these two terms. \mathcal{S} is the function of Softmax. Q , K , and V are the query, key, and value matrices for the attention operation applied to text cross-attention, while K' and V' correspond to cross-modal attention. Given the query features Z and cross-modal semantic features C' , the query matrix Q is defined as $Q = ZW_q$, with $K' = C'W'_k$ and $V' = C'W'_v$. Notably, only W'_k and W'_v are trainable parameters, focusing

Algorithm 1 AnomalyControl Training Algorithm

Data: visual anomaly descriptor I_a , textual anomaly descriptor T_a , anomaly region mask M_A , targeted text prompt T_t , time steps T
Input: Number of training steps T_{train} , Guidance steps T_g
Output: Trained model parameters for AnomalyControl

```

for  $t_{\text{train}} \leftarrow 1$  to  $T_{\text{train}}$  do
    Sample a batch of images  $I$  from the training dataset  $I_a$ 
    Encode images to latent space:  $z = \text{Encoder}(I)$ 
    Sample noise  $\epsilon \sim \mathcal{N}(0, 1)$ 
    Sample time step  $t \sim \text{Uniform}(1, T)$ 
    Add noise to the latent variable  $z$  to obtain  $z_t$ 
    Set trainable attention guidance variable  $e_g = 0$ 
    Extract text embedding  $e_t$  and visual embedding  $e_v$  from the frozen VLM.
    for  $g \leftarrow 1$  to  $T_g$  do
        Generate attention map  $A = \text{VLM}_{\text{crossattn}}(e_t, e_v + e_g)$ 
        Compute average attention map  $\bar{A}_{\text{anomaly}}$  by Eq. 2
        Compute  $E(\bar{A}_{\text{anomaly}}, M_A)$  by Eq. 3
        Update  $e_g$  by Eq. 4
    end
    Generate cross-modal semantic feature  $C' = \text{VLM}(e_t, e_v + e_g)$ 
    Compute loss  $\mathcal{L}$  by Eq. 6
    Backpropagate  $\mathcal{L}$  and update SGA parameters
end
return Trained AnomalyControl model parameters

```

the adaptation on cross-modal information. During training, only the parameters of the SGA and e_g are optimized, while the pre-trained diffusion model and VLM parameters remain frozen. The entire AnomalyControl pipeline is trained on image-text pairs of anomaly images, with a training objective based on the original Stable Diffusion work:

$$\mathcal{L} = \mathbb{E}_{z_t, t, C, C', \epsilon \sim \mathcal{N}(0, 1)} [\|\epsilon - \epsilon_{\theta}(z_t, t, C, C')\|_2^2]. \quad (6)$$

This setup allows the SGA to integrate anomaly-specific semantic signals effectively, ensuring high-quality and controllable anomaly synthesis.

4. Experiments

4.1. Experimental setup

Datasets. We conducted our experiments on the widely used MVTec AD dataset [3, 4], which comprises 5,354 images across 15 categories for industrial anomaly detection tasks, including 10 object categories and 5 texture categories. Each category is represented by a set of defect-free training images and a test set containing images with various defects as well as defect-free images. Pixel-level annotations are provided for all existing anomalies in this

Table 2. Generation quantitative results with IS and IC-LPIPS (abbreviated as IL) on MVTec AD dataset. Bold values indicate the best results, and underlined values indicate the second-best results.

Method	Metric	bottle	cable	caps	carp	grid	hazel	leath	metal	pill	screw	tile	brush	trans	wood	zipper	Mean
DiffAug [39]	IS	1.59	1.72	1.34	1.19	1.96	1.67	2.07	1.58	1.53	1.10	1.93	1.33	1.34	2.05	1.30	1.58
	IL	0.03	0.07	0.03	0.06	0.06	0.05	0.06	0.29	0.05	0.10	0.09	0.06	0.05	0.30	0.05	0.09
CDC [22]	IS	1.52	1.97	1.37	1.25	1.97	1.97	1.80	1.55	1.56	1.13	2.10	1.63	1.61	2.05	1.30	1.65
	IL	0.04	0.19	0.06	0.03	0.07	0.05	0.07	0.04	0.06	0.11	0.12	0.06	0.13	0.03	0.05	0.07
SDGAN [21]	IS	1.57	1.89	1.49	1.18	1.95	1.85	2.04	1.45	1.61	1.17	2.53	1.78	1.76	2.12	1.25	1.71
	IL	0.06	0.19	0.03	0.11	0.10	0.16	0.12	0.28	0.07	0.10	0.21	0.03	0.13	0.25	0.10	0.13
DefGAN [35]	IS	1.39	1.70	1.59	<u>1.24</u>	2.01	1.87	2.12	1.47	1.61	1.19	2.35	1.85	1.47	2.19	1.25	1.69
	IL	0.07	0.22	0.04	0.12	0.12	0.19	0.14	0.30	0.10	0.12	0.22	0.03	0.13	0.29	0.10	0.15
DFMGAN [8]	IS	<u>1.62</u>	1.96	1.59	1.23	1.97	1.93	2.06	1.49	<u>1.63</u>	1.12	2.39	<u>1.82</u>	1.64	2.12	1.29	1.72
	IL	0.12	0.25	0.11	0.13	0.13	0.24	0.17	0.32	0.16	0.14	0.22	0.18	0.25	0.35	0.27	0.20
AnoDiff [13]	IS	1.58	2.13	1.59	1.16	2.04	2.13	1.94	1.96	1.61	1.28	2.54	1.68	1.57	2.33	1.39	1.80
	IL	0.19	0.41	0.21	0.24	0.44	0.31	0.41	0.30	<u>0.26</u>	0.30	0.55	0.21	0.34	0.37	0.25	0.32
AnoXFusion [12]	IS	<u>1.62</u>	2.13	<u>1.68</u>	1.16	<u>2.12</u>	2.24	2.00	1.96	<u>1.63</u>	1.29	2.55	1.80	1.64	2.09	1.37	<u>1.82</u>
	IL	0.19	0.42	<u>0.20</u>	0.22	<u>0.45</u>	0.33	0.42	0.34	0.27	0.29	0.52	0.22	<u>0.36</u>	<u>0.38</u>	0.26	0.33
Ours	IS	1.63	2.14	1.69	1.18	2.26	2.12	2.08	1.98	1.64	1.25	2.53	1.80	<u>1.66</u>	<u>2.20</u>	1.40	1.84
	IL	0.19	0.44	<u>0.20</u>	0.28	0.47	0.35	0.43	0.34	0.27	0.28	<u>0.53</u>	0.24	0.39	0.40	0.26	0.35

dataset. We utilized the captions from MVTec AD Caption [12] for training and testing, which were carefully designed to ensure cross-modal complementarity. For data partitioning, we use the lowest one-third of ID numbers from the anomaly dataset as the training set, with the remaining two-thirds reserved for testing. For each anomaly type, 1,000 pairs of anomaly images and corresponding masks are generated using the mask generation method from AnoDiff [13]. These pairs are employed for downstream anomaly detection and localization tasks.

Metrics. Following previous methods [12, 13], to evaluate the quality and diversity of synthesized anomalies, we used the Inception Score (IS) [30], which measures overall quality and diversity in generated images, and the Intra-cluster Pairwise Learned Perceptual Image Patch Similarity (IC-LPIPS) [23] to evaluate perceptual similarity and the generalization of synthetic anomalies. For evaluating accuracy in downstream tasks such as anomaly detection and localization, we employed measurements through pixel-level and image-level Area Under the Receiver Operating Characteristic Curve (AUROC), Average Precision (AP), and F1-max scores. Consistent with DRAEM[34]’s procedure, we generated 1,000 images per anomaly category and trained a U-Net alongside normal samples.

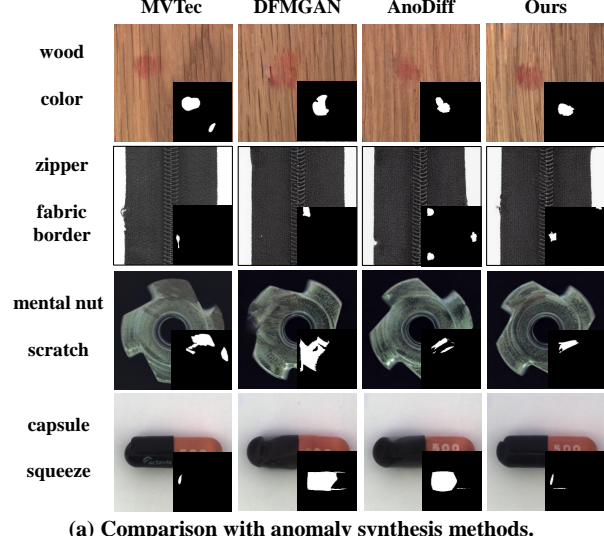
Implementation Details. AnomalyControl is implemented with the HuggingFace Diffusers library [24] and built on the Stable Diffusion 1.5 (SD1.5) model. The VLM utilized in CSM is based on BLIP-2 [16], which provides robust semantic feature extraction for cross-modal inputs. We incorporate a new image cross-attention layer into each of SD1.5’s 16 cross-attention layers, setting the cross-modal

guidance strength parameter $\gamma = 1$ for balanced guidance. The number of guidance steps T_g in ASEA is set to 3. We use the AdamW optimizer [18] with a fixed learning rate of 0.0001 and weight decay of 0.01. For classifier-free guidance, text or cross-modal semantic features are independently dropped with a probability of 0.05, and both are dropped simultaneously with a probability of 0.05. Training is conducted on a single NVIDIA 4090 GPU, requiring approximately three days for 30K iterations. During inference, a 30-step DDIM sampler is used, with a guidance scale of 7.5, to achieve a balance between fidelity and generalization in the generated anomalies.

Baselines. For anomaly synthesis comparisons, we selected several recent high-performing methods as baselines, including DiffAug [39], CDC [22], SDGAN [21], DefGAN [35], DFMGAN [8], AnoDiff [13], and AnoXFusion [12]. To evaluate performance in downstream anomaly detection and localization tasks, we compared our approach with existing outperforming techniques such as DRAEM [34], PRN [36], DFMGAN [8], AnoDiff [13], and AnoXFusion [12].

4.2. Comparison in Anomaly Synthesis

Table 2 illustrates the quantitative results for the generation task on the MVTec AD dataset. Our method achieves the highest average IS of 1.84 and the highest average IL of 0.35, surpassing all other methods in both overall quality and generalization. These results demonstrate our model’s ability to generate high-quality, diverse anomalies that closely resemble real-world anomalies while maintaining robustness across different anomaly types.



(a) Comparison with anomaly synthesis methods.

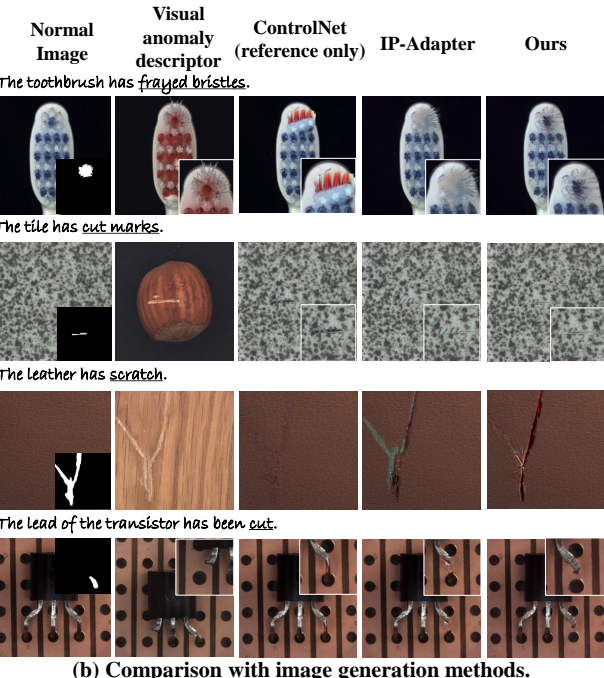


Figure 3. Qualitative Evaluation. It is observed that our method could exhibit large improvements in realism and generalization. (a) Comparison with anomaly synthesis methods. Each row showcases anomalies across various object categories, where binary-value masks indicate the position of the generated anomaly regions. (b) Comparison with image generation methods. From left to right, the columns display a normal image with a mask indicating the target anomaly region, a visual anomaly descriptor to provide visual guidance, and the generated results using different methods (*i.e.*, reference-only mode ControlNet, IP-Adapter, and our method), respectively.

Figure 3 provides a qualitative evaluation of our approach's effectiveness in anomaly synthesis. (a) In com-

Table 3. Results of anomaly detection on MVTec AD dataset. P denotes the results of anomaly localization (pixel-level) and I denote the results of anomaly detection (image-level).

Method	AUC-P	AP-P	F1-P	AUC-I	AP-I	F1-I
DRAEM [34]	92.2	54.1	53.1	94.6	97.0	94.4
PRN [36]	96.9	66.2	64.7	91.6	96.6	92.4
DFMGAN [8]	90.0	62.7	62.1	87.2	94.8	94.7
AnoDiff [13]	99.1	81.4	76.3	99.2	99.7	98.7
AnoXFusion [12]	99.3	86.1	80.6	99.2	99.8	98.7
Ours	99.5	87.4	81.2	99.3	99.8	98.0

parison with anomaly synthesis methods, our approach outperforms existing methods by producing anomalies with enhanced realism, closely aligning with real-world defect patterns. (b) In the comparison with image generation methods, we selected reference images from different categories than the target images (for the first three rows) or from the same category with anomalies in different locations (for the fourth row). This setup demonstrates our method's flexibility in transferring anomalies across various contexts and positions, thereby enhancing the model's generalization capability. Our approach demonstrates superior control over anomaly placement and appearance, accurately capturing the characteristics of the reference anomalies. This improvement in visual fidelity highlights our method's advantage in generating realistic, high-quality anomalies.

4.3. Comparison in Downstream Tasks

As shown in Table 3, our model consistently outperformed other anomaly synthesis methods across most evaluation metrics, demonstrating superior efficacy in both anomaly detection and localization. By enabling fine-grained controls over the appearance of anomalies, our approach can ensure that the generated samples closely resemble real-world defects. This capability is crucial in providing diverse and realistic training data, allowing downstream models to generalize better to real-world anomalies and improve both detection sensitivity and localization accuracy.

4.4. Ablation Study

From the experimental results in Table 4, it is observed that the stepwise introduction of each module significantly improves model performance. First, with only the SGA module, IS and IL increase to 1.66 and 0.23, respectively, while AUC-P and AUC-I reach 92.7 and 95.4. At this stage, the model only uses the visual anomaly descriptor, functioning as an adapter based solely on the image prompt. The addition of the SGA module shows that SGA can strengthen the focus on the anomaly regions in the image. When the CSM module is further introduced, IS rises from 1.66 to 1.69, IL from 0.23 to 0.25, and AUC-P and AUC-I reach 93.1 and 95.8. This improvement indicates that the CSM mod-

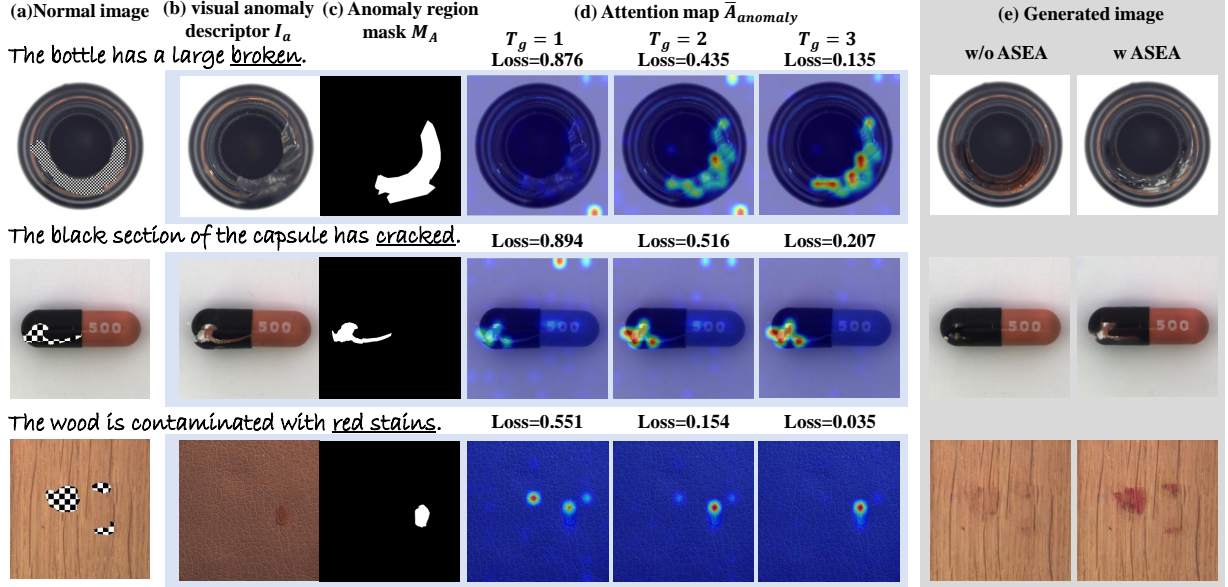


Figure 4. Effect of guidance steps T_g in ASEA. As T_g increases, the loss value is decreased, where ASEA progressively refines VLM’s attention on anomaly regions. The generated images exhibit improved anomaly realism, confirming the effectiveness of ASEA in focusing on specified anomaly regions and producing more visually realistic anomalies.

Table 4. Ablation Study. All modules (CSM, ASEA, and SGA) could improve the effectiveness of the method. We also study the impact of different guidance steps T_g in ASEA.

SGA	CSM	ASEA- T_g	IS	IL	AUC-P	AUC-I
-	-	-	1.50	0.18	90.3	93.0
✓	-	-	1.66	0.23	92.7	95.4
✓	✓	-	1.69	0.25	93.1	95.8
✓	✓	1	1.70	0.25	94.1	96.8
✓	✓	2	1.78	0.28	96.2	97.9
✓	✓	3	1.84	0.35	99.5	99.3
✓	✓	4	1.84	<u>0.33</u>	99.3	99.3
✓	✓	5	1.84	0.35	99.4	99.0

ule incorporates the textual anomaly descriptor, integrating it with the visual anomaly descriptor for cross-modal semantic fusion, thereby improving the quality and coherence of anomaly generation. As described in the methods section, the CSM module captures cross-modal semantic features of the anomaly region through multimodal interactions, resulting in anomaly features that align better with the intended descriptions. Finally, for the ASEA module, different guidance steps T_g demonstrate its impact on model performance. When $T_g = 3$, all metrics reach optimal values, providing the best balance between computational efficiency and performance. Increasing T_g to 4 or 5 shows marginal improvements, indicating that performance gains plateau while computational costs continue to rise. As shown in Figure 4, ASEA progressively refines VLM’s fo-

cus on specified anomaly areas, leading to generated images with higher anomaly realism. This indicates ASEA’s effectiveness in concentrating attention, resulting in visually realistic and detailed anomalies. By enhancing focus on anomaly-specific regions, ASEA effectively helps to generate high-quality, detailed anomaly images.

5. Conclusion

In this paper, we propose an AnomalyControl framework for controllable anomaly synthesis, which enables the flexible generation of realistic and generalized anomaly samples. AnomalyControl introduces two three modules, *i.e.*, Cross-modal Semantic Modeling (CSM), Anomaly-Semantic Enhanced Attention (ASEA), and Semantic Guided Adapter (SGA). To enhance the realism of the synthesized anomalies, CSM aims to extract detailed cross-modal semantic features based on the textual and visual anomaly descriptors, where ASEA could capture fine-grained visual details through multimodal interactions. Then, prompted by precise and controllable instructions, SGA could leverage these enriched semantic signals to guide the diffusion process for high-quality anomaly synthesis. Extensive experiments indicate that AnomalyControl can achieve state-of-the-art results in anomaly synthesis by generating realistic and generalized anomalies based on different control signals and outperforming existing methods for downstream tasks.

References

[1] Omri Avrahami, Ohad Fried, and Dani Lischinski. Blended latent diffusion. *ACM transactions on graphics (TOG)*, 42(4):1–11, 2023.

[2] Yogesh Balaji, Seungjun Nah, Xun Huang, Arash Vahdat, Jiaming Song, Qinsheng Zhang, Karsten Kreis, Miika Aittala, Timo Aila, Samuli Laine, et al. ediff-i: Text-to-image diffusion models with an ensemble of expert denoisers. *arXiv preprint arXiv:2211.01324*, 2022. 2

[3] Paul Bergmann, Michael Fauser, David Sattlegger, and Carsten Steger. Mvtac ad—a comprehensive real-world dataset for unsupervised anomaly detection. In *Proceedings of the IEEE/CVF Conference on Computer Vision and Pattern Recognition (CVPR)*, pages 9592–9600, 2019. 5

[4] Paul Bergmann, Kilian Batzner, Michael Fauser, David Sattlegger, and Carsten Steger. The mvtec anomaly detection dataset: a comprehensive real-world dataset for unsupervised anomaly detection. *International Journal of Computer Vision (IJCV)*, 129(4):1038–1059, 2021. 5

[5] Mikołaj Bińkowski, Danica J Sutherland, Michael Arbel, and Arthur Gretton. Demystifying mmd gans. *arXiv preprint arXiv:1801.01401*, 2018.

[6] Minghao Chen, Iro Laina, and Andrea Vedaldi. Training-free layout control with cross-attention guidance. In *Proceedings of the IEEE/CVF Winter Conference on Applications of Computer Vision (WACV)*, pages 5343–5353, 2024. 5

[7] Ruitao Chen, Guoyang Xie, Jiaqi Liu, Jinbao Wang, Ziqi Luo, Jinfan Wang, and Feng Zheng. Easynet: An easy network for 3d industrial anomaly detection. In *Proceedings of the 31st ACM International Conference on Multimedia (ACM MM)*, pages 7038–7046, 2023. 1, 2

[8] Yuxuan Duan, Yan Hong, Li Niu, and Liqing Zhang. Few-shot defect image generation via defect-aware feature manipulation. In *Proceedings of the AAAI Conference on Artificial Intelligence (AAAI)*, pages 571–578, 2023. 1, 2, 3, 6, 7

[9] Rinon Gal, Yuval Alaluf, Yuval Atzmon, Or Patashnik, Amit H Bermano, Gal Chechik, and Daniel Cohen-Or. An image is worth one word: Personalizing text-to-image generation using textual inversion. *arXiv preprint arXiv:2208.01618*, 2022.

[10] Martin Heusel, Hubert Ramsauer, Thomas Unterthiner, Bernhard Nessler, and Sepp Hochreiter. Gans trained by a two time-scale update rule converge to a local nash equilibrium. *Advances in Neural Information Processing Systems (NeurIPS)*, 30, 2017.

[11] Jonathan Ho and Tim Salimans. Classifier-free diffusion guidance. *arXiv preprint arXiv:2207.12598*, 2022. 5

[12] Jie Hu, Yawen Huang, Yilin Lu, Guoyang Xie, Guannan Jiang, and Yefeng Zheng. Anomalyxfusion: Multi-modal anomaly synthesis with diffusion. *arXiv preprint arXiv:2404.19444*, 2024. 1, 2, 3, 6, 7

[13] Teng Hu, Jiangning Zhang, Ran Yi, Yuzhen Du, Xu Chen, Liang Liu, Yabiao Wang, and Chengjie Wang. Anomalydiffusion: Few-shot anomaly image generation with diffusion model. In *Proceedings of the AAAI Conference on Artificial Intelligence (AAAI)*, pages 8526–8534, 2024. 1, 2, 3, 6, 7

[14] Chaoqin Huang, Aofan Jiang, Jinghao Feng, Ya Zhang, Xinchao Wang, and Yanfeng Wang. Adapting visual-language models for generalizable anomaly detection in medical images. In *Proceedings of the IEEE/CVF Conference on Computer Vision and Pattern Recognition (CVPR)*, pages 11375–11385, 2024. 1

[15] Diederik P Kingma. Auto-encoding variational bayes. *arXiv preprint arXiv:1312.6114*, 2013. 3

[16] Junnan Li, Dongxu Li, Silvio Savarese, and Steven Hoi. Blip-2: Bootstrapping language-image pre-training with frozen image encoders and large language models. In *International Conference on Machine Learning (ICML)*, pages 19730–19742, 2023. 6

[17] Jiaqi Liu, Guoyang Xie, Jinbao Wang, Shangnian Li, Chengjie Wang, Feng Zheng, and Yaochu Jin. Deep industrial image anomaly detection: A survey. *Machine Intelligence Research*, 21(1):104–135, 2024. 1

[18] I Loshchilov. Decoupled weight decay regularization. *arXiv preprint arXiv:1711.05101*, 2017. 6

[19] Chong Mou, Xintao Wang, Liangbin Xie, Yanze Wu, Jian Zhang, Zhongang Qi, and Ying Shan. T2i-adapter: Learning adapters to dig out more controllable ability for text-to-image diffusion models. In *Proceedings of the AAAI Conference on Artificial Intelligence (AAAI)*, pages 4296–4304, 2024.

[20] Alex Nichol, Prafulla Dhariwal, Aditya Ramesh, Pranav Shyam, Pamela Mishkin, Bob McGrew, Ilya Sutskever, and Mark Chen. Glide: Towards photorealistic image generation and editing with text-guided diffusion models. *arXiv preprint arXiv:2112.10741*, 2021. 2

[21] Shuanlong Niu, Bin Li, Xinggang Wang, and Hui Lin. Defect image sample generation with gan for improving defect recognition. *IEEE Transactions on Automation Science and Engineering*, 17(3):1611–1622, 2020. 1, 2, 6

[22] Utkarsh Ojha, Yijun Li, Jingwan Lu, Alexei A Efros, Yong Jae Lee, Eli Shechtman, and Richard Zhang. Few-shot image generation via cross-domain correspondence. In *Proceedings of the IEEE/CVF Conference on Computer Vision and Pattern Recognition (CVPR)*, pages 10743–10752, 2021. 1, 2, 6

[23] Utkarsh Ojha, Yijun Li, Jingwan Lu, Alexei A Efros, Yong Jae Lee, Eli Shechtman, and Richard Zhang. Few-shot image generation via cross-domain correspondence. In *Proceedings of the IEEE/CVF Conference on Computer Vision and Pattern Recognition (CVPR)*, pages 10743–10752, 2021. 6

[24] Patrick von Platen, Suraj Patil, Anton Lozhkov, Pedro Cuenca, Nathan Lambert, Kashif Rasul, Mishig Davaadorj, and Thomas Wolf. Diffusers: State-of-the-art diffusion models. <https://github.com/huggingface/diffusers>, 2022. 6

[25] Alec Radford, Jong Wook Kim, Chris Hallacy, Aditya Ramesh, Gabriel Goh, Sandhini Agarwal, Girish Sastry, Amanda Askell, Pamela Mishkin, Jack Clark, et al. Learning transferable visual models from natural language supervision. In *International Conference on Machine Learning (ICML)*, pages 8748–8763. PMLR, 2021. 3

[26] Aditya Ramesh, Prafulla Dhariwal, Alex Nichol, Casey Chu, and Mark Chen. Hierarchical text-conditional image gener-

ation with clip latents. *arXiv preprint arXiv:2204.06125*, 1(2):3, 2022. [2](#), [3](#)

[27] Robin Rombach, Andreas Blattmann, Dominik Lorenz, Patrick Esser, and Björn Ommer. High-resolution image synthesis with latent diffusion models. In *Proceedings of the IEEE/CVF Conference on Computer Vision and Pattern Recognition (CVPR)*, pages 10684–10695, 2022. [2](#), [3](#)

[28] Olaf Ronneberger, Philipp Fischer, and Thomas Brox. U-net: Convolutional networks for biomedical image segmentation. In *Medical image computing and computer-assisted intervention (MICCAI)*, pages 234–241. Springer, 2015. [3](#)

[29] Chitwan Saharia, William Chan, Saurabh Saxena, Lala Li, Jay Whang, Emily L Denton, Kamyar Ghasemipour, Raphael Gontijo Lopes, Burcu Karagol Ayan, Tim Salimans, et al. Photorealistic text-to-image diffusion models with deep language understanding. *Advances in Neural Information Processing Systems (NeurIPS)*, 35:36479–36494, 2022. [2](#), [3](#)

[30] Tim Salimans, Ian Goodfellow, Wojciech Zaremba, Vicki Cheung, Alec Radford, and Xi Chen. Improved techniques for training gans. *Advances in Neural Information Processing Systems (NeurIPS)*, 29, 2016. [6](#)

[31] Han Sun, Yunkang Cao, and Olga Fink. Cut: A controllable, universal, and training-free visual anomaly generation framework. *arXiv preprint arXiv:2406.01078*, 2024. [2](#)

[32] Zeyue Xue, Guanglu Song, Qiushan Guo, Boxiao Liu, Zhusfan Zong, Yu Liu, and Ping Luo. Raphael: Text-to-image generation via large mixture of diffusion paths. *Advances in Neural Information Processing Systems (NeurIPS)*, 36, 2024. [2](#)

[33] Hu Ye, Jun Zhang, Sibo Liu, Xiao Han, and Wei Yang. Ip-adapter: Text compatible image prompt adapter for text-to-image diffusion models. *arXiv preprint arXiv:2308.06721*, 2023. [2](#), [3](#), [5](#)

[34] Vitjan Zavrtanik, Matej Kristan, and Danijel Skočaj. Draem-a discriminatively trained reconstruction embedding for surface anomaly detection. In *Proceedings of the IEEE/CVF international conference on computer vision (ICCV)*, pages 8330–8339, 2021. [1](#), [2](#), [3](#), [6](#), [7](#)

[35] Gongjie Zhang, Kaiwen Cui, Tzu-Yi Hung, and Shijian Lu. Defect-gan: High-fidelity defect synthesis for automated defect inspection. In *Proceedings of the IEEE/CVF Winter Conference on Applications of Computer Vision (WACV)*, pages 2524–2534, 2021. [1](#), [2](#), [3](#), [6](#)

[36] Hui Zhang, Zuxuan Wu, Zheng Wang, Zheneng Chen, and Yu-Gang Jiang. Prototypical residual networks for anomaly detection and localization. In *Proceedings of the IEEE/CVF Conference on Computer Vision and Pattern Recognition (CVPR)*, pages 16281–16291, 2023. [6](#), [7](#)

[37] Lvmin Zhang, Anyi Rao, and Maneesh Agrawala. Adding conditional control to text-to-image diffusion models. In *Proceedings of the IEEE/CVF International Conference on Computer Vision (ICCV)*, pages 3836–3847, 2023. [2](#), [3](#)

[38] Ximiao Zhang, Min Xu, and Xiuzhuang Zhou. Realnet: A feature selection network with realistic synthetic anomaly for anomaly detection. In *Proceedings of the IEEE/CVF Conference on Computer Vision and Pattern Recognition (CVPR)*, pages 16699–16708, 2024. [1](#)

[39] Shengyu Zhao, Zhijian Liu, Ji Lin, Jun-Yan Zhu, and Song Han. Differentiable augmentation for data-efficient gan training. *Advances in Neural Information Processing Systems (NeurIPS)*, 33:7559–7570, 2020. [1](#), [2](#), [6](#)

[40] Shihao Zhao, Dongdong Chen, Yen-Chun Chen, Jianmin Bao, Shaozhe Hao, Lu Yuan, and Kwan-Yee K Wong. Uni-controlnet: All-in-one control to text-to-image diffusion models. *Advances in Neural Information Processing Systems (NeurIPS)*, 36, 2023. [2](#), [3](#), [5](#)